Investigations of the Influence of Mixture Preparation on Cyclic Variations in a SI-Engine, Using Laser Induced Fluorescence

Johansson, Bengt; Neij, Hans; Aldén, Marcus; Juhlin, Greger

Published in:
SAE Technical Paper Series

1995

SAE TECHNICAL
PAPER SERIES

950108

Investigations of the Influence of Mixture Preparation on Cyclic Variations in a SI-Engine, Using Laser Induced Fluorescence

Bengt Johansson, Hans Neij, Marcus Ald,n, and Greger Juhlin
Lund Institute of Technology

Reprinted from: Engine Combustion and Flow Diagnostics (SP-1090)

The Engineering Society For Advancing Mobility Land Sea Air and Space®
INTERNATIONAL

International Congress and Exposition
Detroit, Michigan
February 27-March 2, 1995

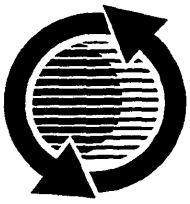

ISSN 0148-7191

Printed in USA 90-1203D/PG

950108

Investigations of the Influence of Mixture Preparation on Cyclic Variations in a SI-Engine, Using Laser Induced Fluorescence

Bengt Johansson, Hans Neij, Marcus Aid,n, and Greger Juhlin
Lund Institute of Technology

ABSTRACT
To study the effect of different injection timings on the charge inhomogeneity, planar laser-induced fluorescence (PLIF) was applied to an operating engine. Quantitative images of the fuel distribution within the engine were obtained. Since the fuel used, iso-octane, does not fluoresce, a dopant was required. Three-pentanone was found to have vapour pressure characteristics similar to those of iso-octane as well as low absorption and suitable spectral properties.

A worst case estimation of the total accuracy from the PLIF images gives a maximum error of 0.03 in equivalence ratio. The results show that an early injection timing gives a higher degree of charge inhomogeneity close to the spark plug. It is also shown that charge inhomogeneity gives a more unstable engine operation. A correlation was noted between the combustion on a cycle to cycle basis and the average fuel concentration within a circular area close to the spark plug center. The correlation coefficient when a second order polynomial was fitted reached a value of -0.8 when the engine operated with a high degree of inhomogeneity. The highest correlation coefficient between the duration of 0-0.5% heat released and the average fuel concentration was obtained within a radius of approximately 5-10 mm from the spark plug. When the standard disc-shaped combustion chamber was replaced with a turbulence generating geometry, the inhomogeneity of the charge became very low, independent of injection timing. No cycle to cycle correlations between fuel/air equivalence ratio and combustion were then noted.

INTRODUCTION

The spark ignition engine operation is to a large extent influenced by the mixture preparation prior to combustion. The mixture preparation has, since the birth of the engine, been one of the key elements enabling a smooth and stable running machine. Nicolaus August Otto, the inventor of the modern four stroke engine, did in fact use three of four known claims on the mixture preparation in the patent of 1876 [1]. The modern engine has in principle the same problems as Otto's first four-stroke. The air/fuel charge injected into the engine cylinder must be prepared to enable a stable operation.

Today most spark ignition engines use pulse-width modulated solenoid valves to inject a quantity of fuel into the engine inlet. Two types of injection systems are common: the single-point type, which uses only one large injector located close to the throttle; and the port type, in which each cylinder is supplied with one smaller injector [2]. The latter type can be operated with several forms of synchronisation to the engine's working cycle. The earliest port-injection systems operated all injectors in parallel and gave one injection per two crankshaft revolutions. In a four cylinder engine this meant that for one cylinder the fuel will be injected against an open inlet valve. Later systems with computer controlled injection, on the other hand used a sequential injection timing. This meant that the injection for each cylinder was phased to a specific cylinder's inlet period.

The use of sequential injection timing gives the engine designer the freedom to decide if the injection should take place during the inlet stroke or not. Injection against an open valve is known to influence the specific fuel consumption as well as the emissions of unburned

hydrocarbons (HC) and nitrogen oxides (NOx) [3]. This influence is caused by the different available mixing times resulting from the injection phasing and hence different charge inhomogenities within the engine cylinder at the time of combustion. An engine with a tumbling cylinder flow pattern is most favoured by injection against closed valves, whereas a swirling motion design is favoured by injection against an open valve [4]. Recent results indicate that injection in the early part of the inlet valve open period is a suitable strategy for reduction of inhomogenities in the cylinder charge [5].

The inhomogenities produced by the injection timing is not necessarily negative. Large scale inhomogenities can be beneficial if it is possible to locate a fuel rich zone close to the spark plug. This zone facilitates a faster and more stable early flame propagation due to a higher laminar flame speed. For an engine operating with a high air excess factor or with much exhaust gas recycling, EGR, this can be very beneficial. The concept of charge stratification with a fuel rich zone close to the spark plug has previously been used in lean burn engines [6]. The use of charge stratification for stabilising the combustion in lean burn engines does, however, require that the cycle to cycle variations in the air/fuel-ratio close to the spark plug be low; otherwise the stability gained from a faster combustion initiation will be lost.

During the last decade studies of combustion processes have been carried out with increasing success using different laser techniques. The main features of the laser techniques are their ability to offer high spatial as well as temporal resolution, in combination with a favourable non-intrusiveness. The Laser-Induced Fluorescence technique offers a great potential for measurements of species concentrations, see e.g. [7-8]. Applications in engines have been successfully carried out, see e.g. [4-5], [9-11].

The aim of the present experiments was to investigate a possible correlation between the variations of fuel/air equivalence ratio, denoted F/A in this work, close to the spark plug and the variation of the combustion. F/A was measured by Laser-Induced Fluorescence from an additive, 3-pentanone, which was seeded to the fuel. Extensive investigations of the validity of using this species as a dopant under engine conditions are also described. To change the deviation of F/A, the injection timing was varied with the use of port injection. A reference condition with a very homogenous charge was obtained by injecting the fuel very far from the engine inlet.

STRATEGIES FOR FUEL VISUALISATION ENGINES USING LIF

The fuel used in this study was iso-octane. Because of the absence of fluorescence from iso-octane, [12], it needed to be seeded with a fluorescing additive. This additive was sought among previously used flowfield tracers such as acetaldehyde [13-14], acetone [15], biacetyl [16-17] and TMPD [18-19] and 3-pentanone [9-12].

Apart from having suitable fluorescent properties, the dopant must also follow the fuel. The dopant must be soluable in the fuel and their vaporization characteristics must be similar [20]. Acetaldehyde, acetone and biacetyl were excluded as dopants because of differences in vaporisation characteristics as compared to those of iso-octane, see Figure 1. TMPD was excluded because of its strong dependence on oxygen concentration through quenching. As indicated in Figure 1, the vaporisation characteristics of 3-pentanone are similar to those of iso-octane.

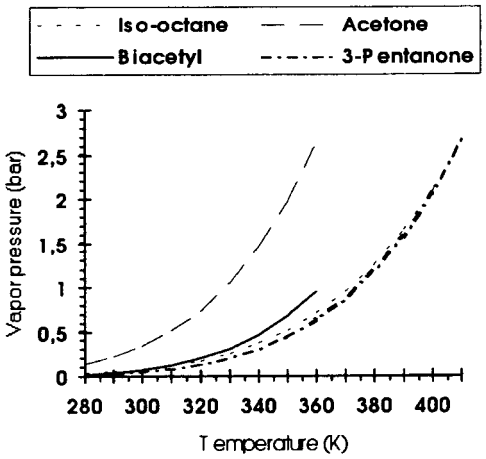

Figure 1 Dependence of vapour pressure on temperature for iso-octane, acetone, biacetyl and 3-pentanone, based on data from [21]. No data has been found for biacetyl at pressures above one atmosphere.

In Table 1 are given the coefficients of vapour phase mass diffusion in air for the possible dopants at conditions that are comparable to those in the intake pipe where the fuel/dopant mixture is injected into the air. A rather close similarity between iso-octane and 3-pentanone can be observed.

Due to the similarity between iso-octane and 3- pentanone in terms of vapour pressure and molecular diffusion coefficient, 3-pentanone was chosen as dopant.

Table 1: The molecular coefficients of vapour phase mass diffusion (10^{-6} m^2/S) in air at a pressure of 1 bar and a temperature of 373 K.

Iso-octane	10.0
Acetone	15.6
3-pentanone	12.4
Acetaldehyde	18.3
Biacetyl	13.5

Three-pentanone, $C_2H_5COC_2H_5$, has an absorption spectrum ranging from 220 nm to 330 nm with a peak at 280 nm. The emission spectrum range is 330 nm to 600 nm with a peak at 430 nm [22]. The fluorescence quantum yield is found to be essentially independent of excitation wavelength [22], measured in a cell where 10.0 torr 3-pentanone was mixed with 2.0 torr O_2.

The validity of the results when adding 3-pentanone to iso-octane for LIF measurements was further tested in the actual experimental environment, i.e. in the running engine. For these fundamental investigations the engine was fuelled with a homogeneous charge created by fuel injection far from the engine. Excitation was performed at 248 nm using a KrF excimer laser.

Power dependence - The power dependence was measured for excitation energies from 10 mJ to 100 mJ. A plot of the signal strength vs. excitation energy was linear, i.e. the fluorescence intensity was found to be directly proportional to the laser intensity.

Quenching - Strong quenching of the fluorescence by oxygen would have been detrimental to the measurements. Therefore, laboratory cell measurements were conducted where the lifetime of 3-pentanone surrounded by pure nitrogen gas was compared to that of 3-pentanone in air [23]. The measurements were carried out at a wavelength of 266 nm. Small, if any, differences were found; the measured lifetime for 100 mbar 3-pentanone in 9.2 bar nitrogen gas, or air, at 523 K was 2.6±0.25 ns.

Concentration linearity - In the engine the fluorescence intensity was monitored as a function of F/A with the iso-octane fuel doped with 2% 3-pentanone. The result is shown in Figure 2. The LIF signal was found to be directly proportional to the injected amount of fuel, at least up to the investigated F/A of 0.8. Because of knocking, the engine could not be run on a higher F/A than 0.8.

Absorption - Over the field of view, 20 x 30 mm^2, the calculated absorption was less than 0.5%. The molar absorption coefficient for 3-pentanone at 248 nm, 5.3 $M^{-1}cm^{-1}$ was found in the absorption spectrum [22].

Flame speed influence - The possible influences on the flame speed from the additive was investigated by comparing the heat release data from an engine running on either pure iso-octane or on iso-octane with 2% and 5% added 3-pentanone, respectively. No changes in flame speed were observed. No experimental investigations have been found in the literature on flame speed changes by addition of additives to iso-octane. There is, however, a report on a maximum flame speed increase of 3% for lean/stoichiometric combustion, when 5% methyl ethyl ketone, $CH_3COC_2H_5$, closely related to 3-pentanone, was added to propane [24].

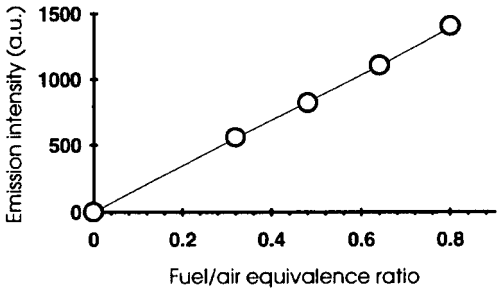

Figure 2 Dependence of the fluorescence intensity on fuel concentration, 2% 3-pentanone in iso-octane.

Decomposition of 3-pentanone - During the measurements it was observed that the fluorescence signal level from the 3-pentanone/iso-octane mixture was stronger immediately after the preparation of the mixture than it was several hours later. This signal decline was attributed to decomposition of the 3-pentanone in the iso-octane. Since the total time of the measurements was 13 minutes for the different fuel injection timings, this was not a problem.

EXPERIMENTAL ARRANGEMENT

A rough outline of the experimental set-up is shown in Figure 3. A tuneable KrF excimer laser (Lambda Physik EMG 150 MSC) with a maximum pulse energy of 250 mJ at 248 nm was used. The laser beam was formed to a sheet, 0.1 x 12 mm^2, using cylindrical lenses, and focused into the engine. The laser energy was approx. 100 mJ/pulse. The total laser intensity was monitored on a pulse-to-pulse basis by measuring the power of the laser beam after its passage through the combustion chamber. This was done by a power meter, Lambda Physik SN 1044M, which yielded a signal proportional to the incident laser energy (2.5 V/J). The camera detector controller had the option of registering a signal that is externally fed to the system, and saved this information in the first column of a simultaneously acquired image.

The fluorescence was collected at right angles from the laser sheet by a NIKKOR 50 mm, f/1.2 lens. As detector, a gateable, image-intensified CCD camera, Princeton Instruments ICCD-576S/RB-T, consisting of 384 x 576 pixels, each 23 æm squared was used. The imaged area inside the combustion chamber was 30 x 20 mm^2. By investigation of the individual hardware pieces, i.e. the lens system, the image intensifier and the CCD detector, a resulting image resolution was measured to 2.5 pixels,

corresponding to approx. 125 μm [12]. Unwanted laser scattering was eliminated by coloured filters in front of the detector. The ICCD camera and the laser were triggered by pulses from the crank shaft encoder. This device monitors the position of the crank shaft and sends 1800 pulses during one revolution. The temporal resolution of the triggering, for an engine speed of 700 rpm, was 47.6 μs. The laser firing and the camera exposure was set to one crank angle degree before ignition. The gating time of the fluorescence detection system was fixed at 100 ns.

The ignition system used was of the inductive type, with a spark duration of approximatly | ms [13]. A commercially available spark-plug with extended electrodes was used, NGK BCRE527Y. It was mounted in the centre of the cylinder head. Because of the risk for laser light reflections from the spark plug, the laser light focus was approx. 1.5 mm from the spark plug. The distance from the center of the spark gap to the laser sheet was ~3 mm, see Figure 3. The laser sheet was placed in front of the electrodes. A reduction in the amount of scattered light from the spark plug could be obtained by placing the laser sheet behind the electrodes. This approach was not successful as the electrodes themselves decreased the accessible solid angle, i.e. the light collecting efficiency, in the measurement region near the spark gap.

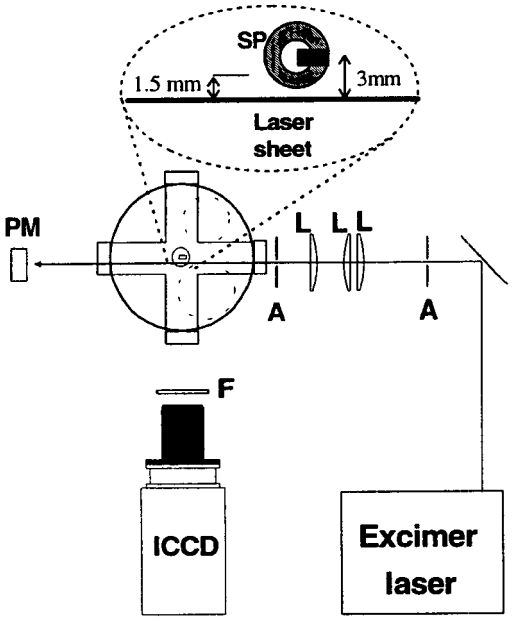

Figure 3 Experimental set-up. The positions of the spark plug and the inlet and exhaust valves are indicated. L: cylindrical lens, A: aperture, F: filter, PM: power meter, SP: spark plug.

The measurements were performed in a single- cylinder spark-ignition engine based on a six-cylinder VOLVO TD 102 Diesel engine. The top of one of the cylinders was extended by a spacer with three square, high quality, fused silica windows (dimensions 38x38 mm2, thickness 21 mm). The spacer was uncooled and was not to reach a temperature higher than 140øC. Thereby the time of each measurement series was limited to 15-20 minutes. In order to maintain a reasonable compression ratio, the piston was also extended. Two different piston extender configurations were used; one flat piston extender, generating a disc-shaped combustion chamber, and one piston extender with two orthogonal traces drilled into the head, giving a so-called high squish combustion chamber, see Figure 4. The piston extenders were blackened through anodising in order to reduce any background noise from scattered fluorescence inside the combustion chamber.

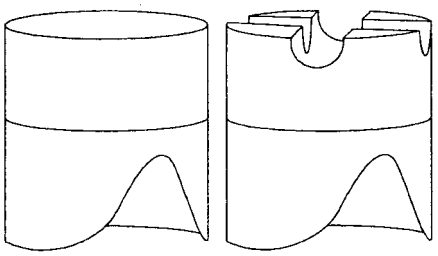

Figure 4 Left: Flat piston extender; Right: High squish piston extender, where two orthogonal traces have been drilled in the top.

The engine was run on iso-octane (purity 99.5%). When a homogenised fuel/air mixture was desired, the fuel was injected into the intake air more than 3 m from the intake port. To further improve the mixing, a 16 dm^3 mixing tank was placed between this injection point and the engine intake. During the fuel visualisation experiments the amount of residual gas should be confined to a low level. The reason for this is that the influence of other causes of cycle to cycle variations should be eliminated. This was achieved by running the engine in a *skip-fire mode*. The engine was run with combustion for 7 cycles and was motored without combustion for another 3 cycles to purge the cylinder of all residual gas. The measurements were performed in the first clean cycle with combustion. Further engine specifications are given in Table 2.

The accumulation of deposits on the windows, in particular on the imaging window, was avoided by heating the intake pipe to 100 °C. The intake air was additionally heated to 90-100 °C by a 3 kW fan. Thanks to these precautions, the engine could be run for an entire day without cleaning of the windows.

Cylinder pressure measurements- The cycle to cycle variations in combustion were monitored by recording the Pressure development. This was done with a piezoelectric transducer, AVL QC42, connected to a Kistler 5001 charge amplifier. The charge amplifier voltage output was connected to a 486/66 PC with a Data Translation DT2823 100 kHz 16-bit A/D-card. A more detailed description can

be found in [26]. To extract information on the early flame development a cycle-resolved heat release calculation was performed on the pressure registrations. The actual amount of heat released during combustion was calculated by using fundamental thermodynamic relations. This is described in [26].

Table 2: Engine specifications.

Displaced volume	(cm^3)	1600
Bore	(mm)	120.65
Stroke	(mm)	140
Connection rod	(mm)	260
Compression ratio, flat piston, liquid fuel		7:1
Compression ratio, high squish, all fuels		10:1
Swirl number		~2.8
Engine speed	(rpm)	700
Inlet valve opening		35 CAD BTDC
Inlet valve closing		78 CAD ABDC
Exhaust valve opening		48 CAD BBDC
Exhaust valve closing		14 CAD ATDC

PROCESSING OF IMAGES

The output images of the fuel distributions had to be processed after acquisition to yield quantitative data. An illustration of the image processing procedure is given in Figure 5. The necessary data for the processing can be summarised as:

- average background image,
- average laser mode cross-section,
- pulse-to-pulse information on the emitted laser energy.

The background image was obtained by motoring the engine. Normally, the background image was homogeneous enough to allow the subtraction of the background image to be replaced by a subtraction of a constant value.

The laser mode cross-section was taken from images of homogeneous fuel distributions that had been accumulated to minimise noise. A section of the accumulated image was added row by row in the direction of the laser sheet, yielding an array containing the spatial laser intensity distribution across the laser sheet.

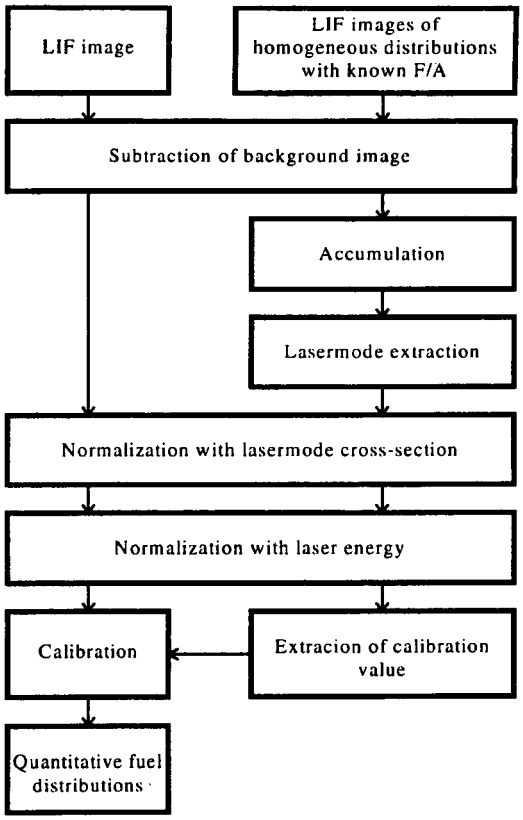

Figure 5 A schematic illustration of the image processing procedure.

The output data of the fuel distributions were saved in one file per experimental run. Customised software was necessary for processing the large amounts of data, see Figure 5. The software was designed to prepare the raw data images for further extraction of quantitative data. After the initial processing, the images contained the actual LIF signal from the doped fuel. This signal could in turn be converted into fuel concentration by relating it to the signal level in images of a known fuel concentration field. In connection to every measurement, measurements of homogeneous fuel distributions were made. These distributions were already used for the extraction of the laser mode cross-section as described above. By using conventional exhaust gas analysis, where the composition of the exhaust gas is related to the fuel/air equivalence ratio fed to the engine [26], the Laser-Induced Fluorescence intensity in these homogeneous distributions could be assigned the corresponding value in terms of the equivalence ratio. The images were accumulated and adjusted with respect to the laser mode cross-section and the total laser energy. The mean value in a section of the homogeneous image was used as a calibration value for all other images taken during the same measurement sequence.

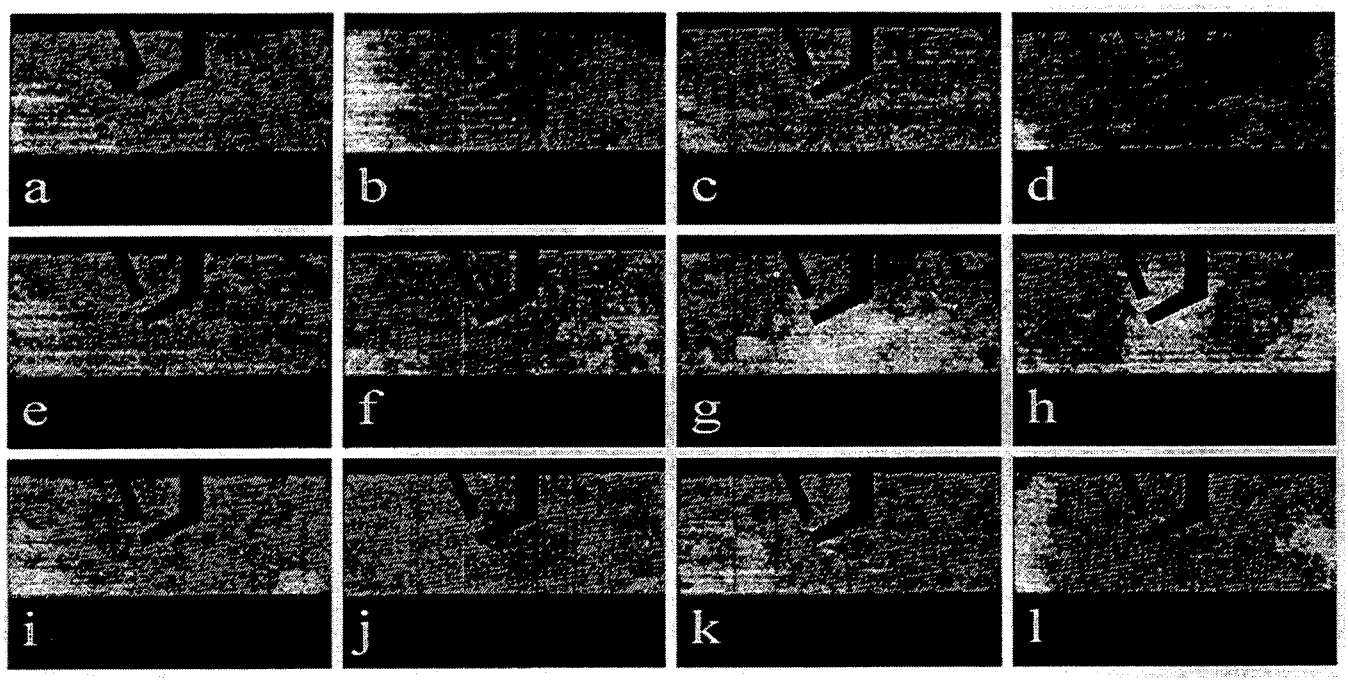

Figure 6: Twelve subsequent fuel distributions measured one CAD prior to ignition.

After this operation the images depict the actual fuel/air equivalence ratio measured prior to ignition in the engine. Due to problems with scattered light from the spark plug, the area in front of the electrodes were excluded before the evaluation. Examples of two-dimensional fuel distributions captured in the engine, run with the flat piston extender, can be studied in Figure 6, where processed measurements from twelve subsequent cycles are displayed. Strong inhomogenities are undoubtedly present.

EVALUATION PROCEDURE

In order to verify the influence of different injection timings, it was necessary to state if any correlation at all existed between image data and engine performance. This was done by:

1. Calculating the mean value around the spark plug within a circular area.
2. Calculating the standard deviation around the spark plug within a circular area.

The mean equivalence ratio is physically relevant through its ability to influence the flame development. The standard deviation, on the other hand, does not have any immediate physical relevance. It can be seen as a global measure of the degree of inhomogeneity. However, it does not give any information on the actual distribution, i.e. an infinite number of distributions may lead to an identical value of the standard deviation.

The mean value and standard deviation within a circular area with its centre in the spark gap were calculated for each image. The radius of the circular area was gradually increased. The mean value and standard deviation within each radius were stored in separate files. A measurement sequence typically consisted of 50 images taken in 50 engine cycles. The described procedure was repeated for each of the 50 images. Naturally, before performing the data extraction, the images were processed and calibrated according to the procedures described in the section *Processing of images* above. For each measurement sequence, finally, three data files were at hand; one containing the heat release data computed from the pressure registrations, the other two containing the equivalence ratio and the standard deviation as a function of radius.

RESULTS

The results of the measurements are given below. The notation F/A denotes the normalised fuel/air equivalence ratio. For a description of how F/A is evaluated, the reader is referred to the section Processing of images above.

HOMOGENEOUS CHARGE - To calibrate the image intensity with the actual fuel/air equivalence ratio, reference conditions with a very well mixed charge were used. Figure 7 below, shows the mean value and standard deviation of average F/A within circles of increasing radius for 50 individual cycles. The variation in F/A is extremely small and an accurate calibration is thus possible.

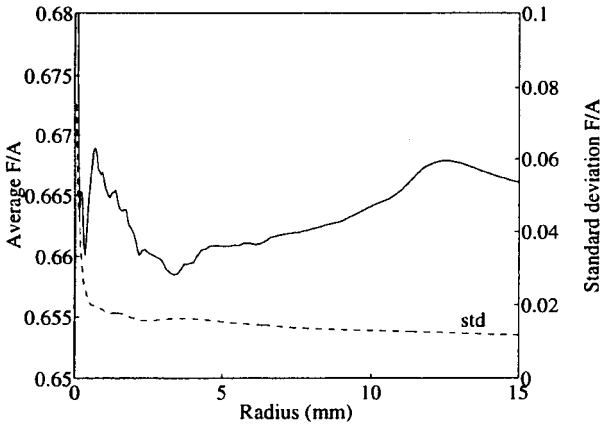

Figure 7 Average F/A and standard deviation in F/A for a homogeneous charge.

INVESTIGATION OF F/A AT DIFFERENT INJECTION TIMINGS - To clarify whether fuel injection against open or closed inlet valve gives the most homogeneous charge in our swirling engine geometry, measurements of F/A were done for three different injection timings, with closing times at 0, 325, and 375 CAD ATDC. For all runs the injection pulse width was set to 12 ms, corresponding to 50 CAD at the operating speed of 700 rpm. For each injection timing, two independent measurement series of 50 cycles each were acquired.

Mean F/A - The mean F/A-values are shown in Figures 8-10. As can be seen, there are no discernible differences in fuel concentration for different radii. What also can be seen is that repetitive values are given with injection valve closings at 0 and 325 CAD ATDC whereas a closing time at 375 CAD ATDC gives a significantly richer result in one of the two engine runs.

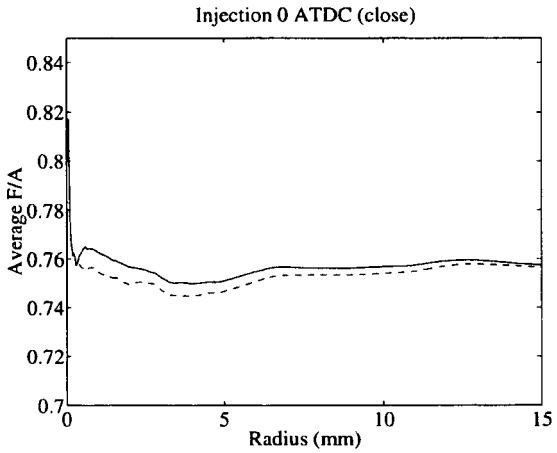

Figure 8 Mean F/A as a function of radial distance from the spark plug. Injection closing at 0 CAD. Two individual engine runs are shown.

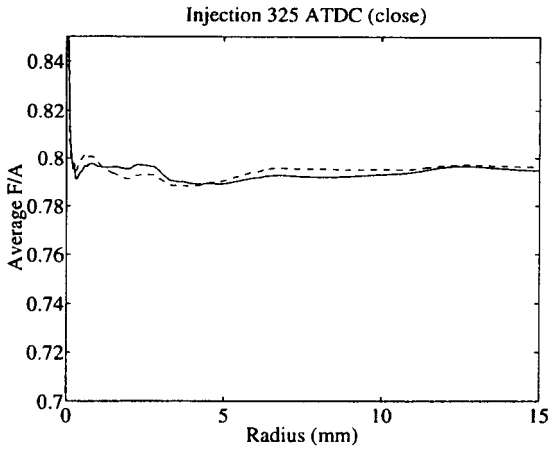

Figure 9 Mean F/A as a function of radial distance from the spark plug. Injection closing at 325 CAD A TDC. Two individual engine runs are shown.

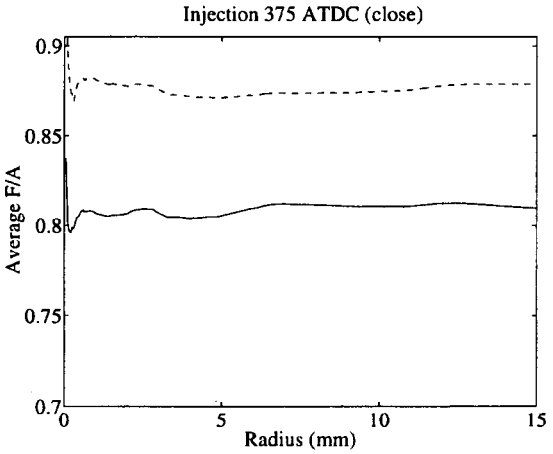

Figure 10 Mean F/A as a function of radial distance from the spark plug. Injection closing at 375 CAD ATDC. Two individual engine runs are shown.

Figures 8-10 are summarised in Table 3, where the mean F/A values are shown. A later injection timing gives a richer mean value of F/A close to the spark plug.

Table 3: Mean F/A for different injection timings.

Injection close (ATDC)	Mean F/A
0	0.76
325	0.8
375	0.82-0.86

Variations in F/A - The variations of the fuel/air concentration can be expressed in different ways. One measure of the variations would be the standard deviation of F/A within a certain radius. This type of evaluation has previously been used to detect effects of injection timings on charge homogeneity [4], but for the present

experimental set-up this kind of evaluation is hazardous as the image intensifier of the ICCD has a high noise level. The inhomogeneity of a cylinder charge, defined as the standard deviation for an image divided by average F/A, will not be low even for a well mixed charge due to this noise. Table 4 shows the average inhomogeneity of a homogeneous charge and the three injection timings.

Another way of expressing the variation of F/A is to look at the variations of average fuel concentration from cycle to cycle. This standard deviation normalised by the mean F/A, denoted COV(F/A), is also shown in Table 4 for the different engine runs. The homogeneous charge here shows a very low standard deviation and hence that a stable engine operation can be expected.

Table 4: Inhomogeneity and cycle to cycle variation of F/A close to spark plug.

Injection time	Inhomogeneity	Cycle to cycle COV(F/A)
ATDC	%	%
0	16.4	9.9
0	15.7	8.2
325	14.6	7.5
325	14.5	6.3
375	15.3	5.1
375	12.6	5.5
homogeneous	12.0	2.0

The standard deviation of F/A for three different injection timings are shown in Figures 11-13, where the mean fuel concentration for each cycle was evaluated in circles with increasing radii. As can be seen, two runs with identical injection timings give approximately the same results. A trend in the figures is a decrease in standard deviation with increasing radius. This decrease is probably the result of the increased number of pixels in the evaluation as the radius increases, but the averaging out of small scale inhomogenieties also contribute.

Figure 14 shows the standard deviation for F/A as a function of injection timing. Early injection causes a high standard deviation of mean F/A.

The rate of early flame propagation is known to be very sensitive to the laminar flame speed. The laminar flame speed in turn has a dependence on F/A. It is then expected that a large spread of F/A close to the spark plug will result in larger variations in the early flame development. Figure 15 shows the standard deviation in the crank angle position of 0.5% heat released as a function of the standard deviation of F/A. The figure shows, as expected, that a large deviation in F/A leads to a large deviation in the early part of the combustion.

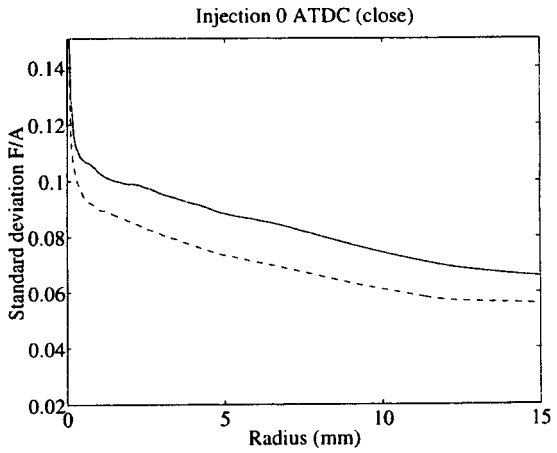

Figure 11 Standard deviation in F/A as a function of radial distance from the spark plug. Injection closing at 0 CAD. Two individual engine runs are shown.

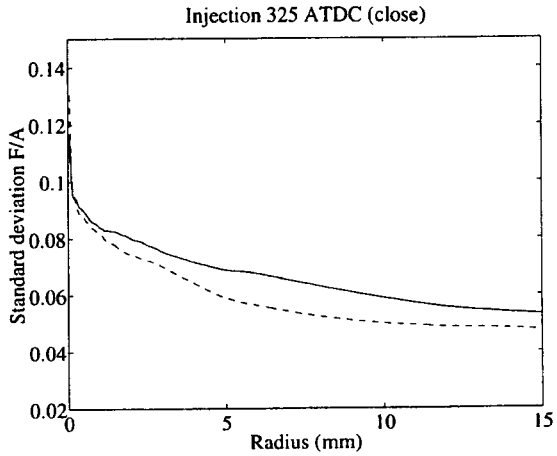

Figure 12 Standard deviation in F/A as a function of radial distance from the spark plug. Injection closing at 325 CAD ATDC. Two individual engine runs are shown.

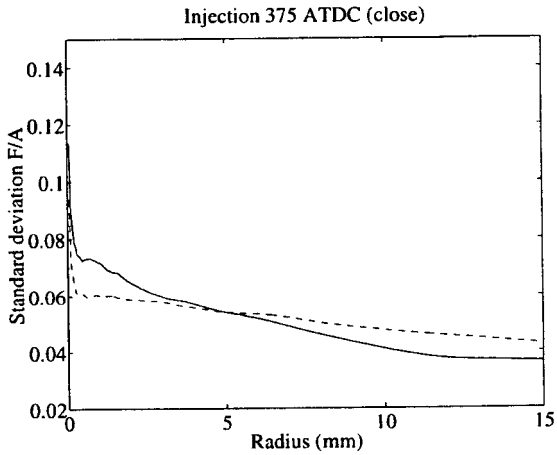

Figure 13 Standard deviation in F/A as a function of radial distance from the spark plug. Injection closing at 375 CAD ATDC. Two individual engine runs are shown.

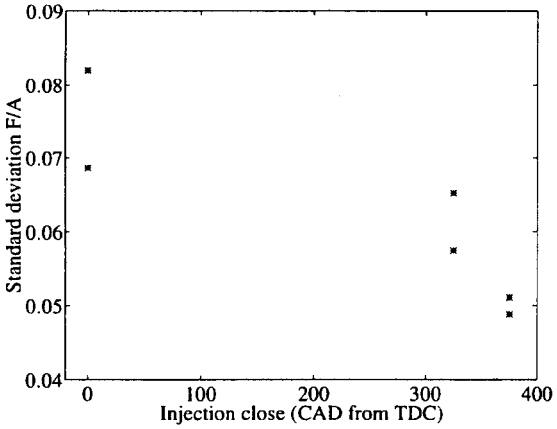

Figure 14 Standard deviation in F/A as a function of injection timing.

The standard deviation of average fuel concentration is not only an effect of the charge inhomogeneity. If the total amount of fuel that enters the cylinder varies from cycle to cycle, this will also give rise to a fluctuation. To detect if there was a cycle to cycle variation in the fuel supply, the COV of the total amount of released heat was plotted against the standard deviation of F/A, see Figure 16. The figure shows that only small variations in heat released are present and hence the same amount of fuel entered the cylinder from cycle to cycle. The figure also shows a lack of correlation between the variation in the total amount of fuel that enter the cylinder and the variations in local F/A close to the spark plug. This implies that the major reason for the increased instabilities from operating the engine with early injection timing are the result of increased charge inhomogeneities in the cylinder.

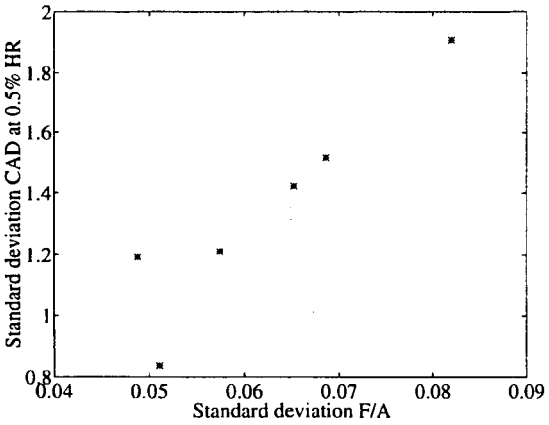

Figure 15 Standard deviation in position of 0.5 % heat released as a function of std(F/A).

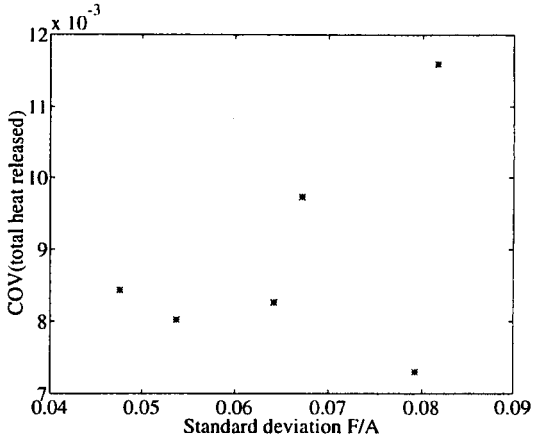

Figure 16 COV of total heat released as a function of standard deviation in F/A.

CYCLE TO CYCLE CORRELATIONS - In order to investigate the correlation of image data to heat release data a statistical evaluation was performed.

Sometimes it is of interest to examine the influence that some variables exert on others. Often the functional relationship that exists is too complicated to be described in simple terms. In this case it is desirable to approximate this function with a simple mathematical function, such as a polynomial. By examining such a function we may be able to appreciate effects produced by changes in certain important variables. The unknown parameters are estimated with the help of available data, and a fitted equation is obtained.

In this case the data was fitted to a second-order polynomial since the laminar burning velocity is known to present an approximate second-order dependence on the equivalence ratio. For a general relationship between two variables x and y it can be written:

$$y_i = \beta_0 + \beta_1 x_i + \beta_2 x_i^2 + \varepsilon_i ,$$

or in matrices

$$Y = X\beta + \varepsilon$$

where
y = a general response variable
x = a general predictor variable
β = regression coefficient
ε = error.

Minimising the sum of squares of deviations from the true line yields b, which is an estimate of β. In matrices this can be expressed as [28]

$$b = (X^T X)^{-1} X^T Y .$$

The multiple correlation coefficient is given by [28]

$$R = \sqrt{\frac{b^T X^T Y - n\bar{Y}^2}{Y^T Y - n\bar{Y}^2}}.$$

The combustion in the engine is characterised by the heat release data. The crank angle position for a certain level of beat release was chosen as the combustion parameter. The crank angle position of, for instance, 0.5% heat released is a measure of the rate of combustion from ignition to the crank angle for 0.5% heat released.

The response and predictor variables for this example would then be

$$Y = \begin{bmatrix} CA_{0.5\%}(1) \\ \vdots \\ CA_{0.5\%}(n) \end{bmatrix},$$

$$X = \begin{bmatrix} 1 & (F/A)_{radius}(1) & (F/A)_{radius}^2(1) \\ \vdots & \vdots & \vdots \\ 1 & (F/A)_{radius}(n) & (F/A)_{radius}^2(n) \end{bmatrix}.$$

A regression analysis was performed for every radius, recalling that the fuel/air ratio was computed within circular areas outwards from the spark gap.

In Figure 17 a data scatter plot is given for the radius yielding the highest cycle to cycle correlation of the position of 0.5 % heat released to mean F/A.

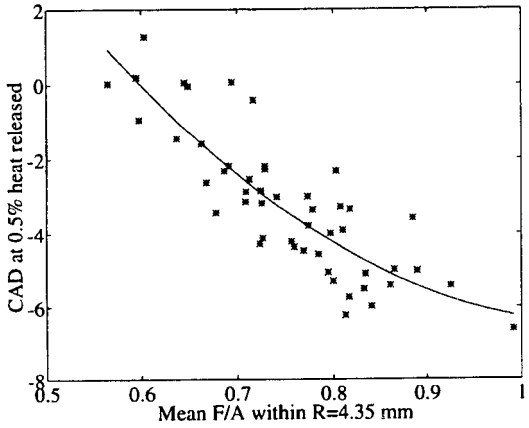

Figure 17 Data scatter plot for the radius yielding the highest correlation between CA 0.5 % heat released and mean F/A.

In Figure 18 the cycle to cycle correlation of CA 0.5% HR to F/A is given as a function of radial distance from the spark plug. The maximum correlation is found at the radius 4.35 mm from the spark plug. Since the highest correlations are obtained from about 4 to 10 mm radius, this implies that F/A structures on the order of one centimeter are responsible for the major part of the increased combustion instability in the early part of the combustion in this engine.

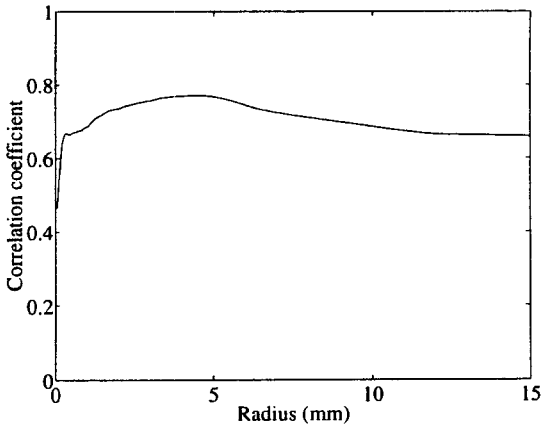

Figure 18 Correlation coefficient as a function of the radius.

In Figures 19-21 are shown the maximum correlations for F/A to different combustion parameters for the three different injection timings investigated. In every figure the results of two independent runs are shown. The abbreviations are explained in Table 5.

The figures show that a cycle to cycle correlation can be found between the fuel concentration in the vicinity of the spark plug and several engine operating parameters. For most engine runs the maximum correlation is obtained between the position of 0.5% heat released and F/A. This is not surprising, since the local fuel concentration is expected to exert the greatest influence on the very early combustion.

The levels of correlation for the three injection timings are different. The earliest injection gives the highest correlation. The reason for this can be found in the different standard deviations of F/A that the injection timings produce, see Figure 14.

Table 5: Explanation of abbreviations used in Figs 19-21

Pmax	Maximum delivered pressure
Pm pos	CA position at maximum pressure
dQmax	Maximum heat release rate
dQ pos	CA position at maximum heat release
Q tot	Total heat released in cycle
0.5	CA Position 0.5 % heat released
1 %	CA position 1 %heat released
2 %	CA position 2 % beat released
5 %	CA position 5 % heat released
10%	CA position 10 % heat released
50%	CA position 50 % heat released
90%	CA position 90 % heat released
95%	CA position 95 % heat released
IMEP	Indicated mean effective pressure

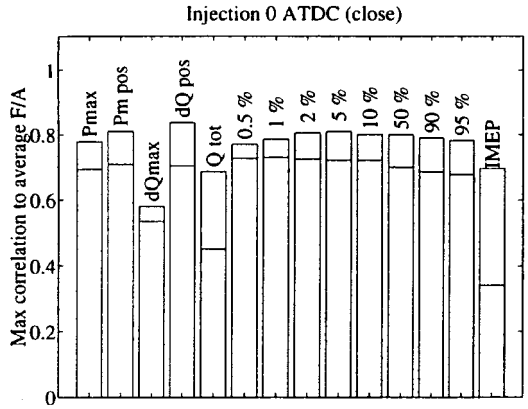

Figure 19 Correlation between F/A and different combustion parameters, injection at 0 CAD.

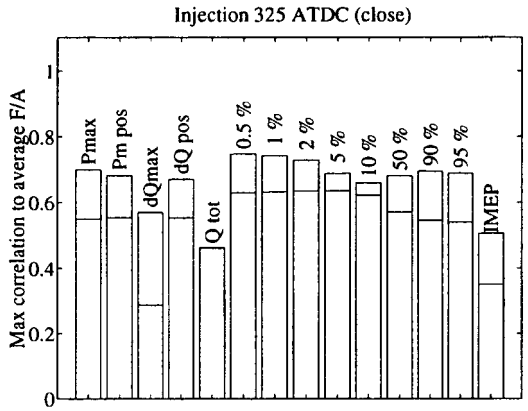

Figure 20 Correlation between F/A and different combustion parameters, injection at 325 CAD.

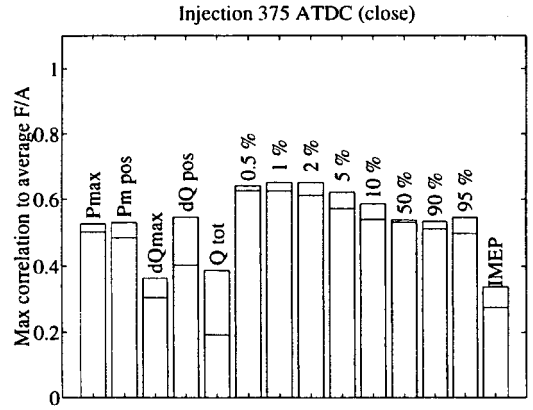

Figure 21 Correlation between F/A and different combustion parameters, injection at 375 CAD.

THE INFLUENCE OF THE COMBUSTION CHAMBER SHAPE - The results presented above were obtained with a disc-shaped combustion chamber, see Figure 4. This geometry gives an undisturbed flow pattern during the compression stroke and consequently a low level of turbulence. The low level of turbulence reduces the possibilities for turbulent diffusion. Inhomogeneities introduced during the inlet phase can then remain even after the entire compression stroke.

If a combustion chamber geometry with a higher level of turbulence is used, the turbulent diffusion will level out the inhomogenities during the compression. To study the effect of combustion chamber shape on the inhomogeneities a high-squish piston extender was used, see Figure 4. This geometry has previously shown a higher level of turbulence [26]. Table 6 shows typical values of the image inhomogeneities, i.e. the mean normalised standard deviation in the images from a measurement sequence, for the flat and the high-squish piston extender, respectively. Table 6 also illustrates typical values of the variation in the mean equivalence ratio within a certain radius from the spark gap in the images (in this case -10 mm), denoted COV(F/A).

Table 6: A comparison between typical values of the inhomogeneity and COV(F/A) for the high-squish and flat piston extender, respectively.

	Inhomogeneity		**COV(F/A)**	
	High-squish	Flat	High-squish	Flat
Homogeneous charge	9-10%	9 - 10%	2%	2%
Inhomogeneous charge	10%	14-15%	4%	12%

From the table it can be seen that the high-squish piston extender produces very homogeneous fuel/air mixtures, ones comparable, in fact, to those obtained from careful premixing of the fuel and the air by fuel injection far from the engine intake pipe. Additionally, the variations in the mean equivalence ratio near the spark plug are small for the high-squish piston. For the flat piston extender both the image inhomogeneity and the non-reproducibility of the mean equivalence ratio near the spark gap are significantly increased.

DISCUSSION

ESTIMATED PRECISION AND ACCURACY OF THE RESULTING IMAGES - In order to evaluate the obtained results, it is of crucial importance to investigate the sources of errors in terms of precision and accuracy. The precision of the images is determined by the image noise, which can be characterised by different parameters. The main noise contributions come from the image intensifier in the detection system and the pulse- to-pulse

spatial variations in the laser sheet. Experiments using a homogeneous fuel distribution have shown that the sum of these two effects yields a total imprecision of ~10%. The measurements were performed using approx. 2% (v/v) 3- pentanone in iso-octane, yielding a single-shot intensity of ~30% of the full dynamic range of the detector. There is thus only a minor contribution from image background noise.

In estimating the accuracy during engine conditions, the temperature and pressure dependencies of the LIF signal must be known. However, the pressure and temperature variations at the ignition time in the engine are very small, less than 1%, and are not liable to introduce uncertainties. Furthermore, recent laboratory experiments in a high pressure-high temperature cell also indicate that the LIF signal from 3-pentanone shows a weak temperature and pressure dependence in the region of interest [23], which means that the errors introduced by these effects are negligible.

As discussed above the absorption over the field of view is less than 0.5% for a homogeneous, stoichiometric fuel/air mixture, and can also be omitted as a source of error. It was also verified that no background level built up in the engine during the measurements. A gradually accumulating background level would have deteriorated the measurements by the continuous addition of an unknown signal level to the actual signal from the fuel. The background level could, however, be checked by motoring the engine, i.e. running it without fuel injection and combustion. These background images were also identical to images taken when running the engine on natural gas, which does not fluoresce after excitation at 248 nm. The ratio of the fluorescence signal to the background level was better than 15. An estimation based on the actual signal levels indicate that if the used background level is a 50% underestimation (worst-case) of the real level, the resulting underestimation of the fuel/air equivalence ratio will be less than 0.02.

The fact that the LIF signal from the 3-pentanone/iso-octane mixture presented a linear concentration dependence in the engine shows that effects of oxygen quenching need not be considered, which also has been confirmed by laboratory lifetime measurements [23]. Errors may also have been introduced through inaccuracy in the calibration value measured by the exhaust gas analysis equipment. However, the inaccuracy of this instrument does not exceed 0.01 in terms of fuel/air equivalence ratio. In conclusion, a maximum, worst-case, underestimation of the equivalence ratio of #0.03 is expected.

ESTIMATION OF MEAN BURNING SPEED - By estimating the burning speed from the image and heat release data, the calculated data can be compared with what can be expected. The burning speed, S_b, can be calculated as

$$S_b = C_\tau \cdot \frac{r_{F/A-mixture}}{CA_{0.5\%} - CA_{ign}},$$

where C_r, is a constant, converting crank angle degrees into seconds, r is the radius of a sphere containing the mass unhurried F/A corresponding to 0.5% heat released, the so-called equivalent flame radius. The equivalent flame radius can be calculated as [27]

$$r = \sqrt[3]{\frac{3}{4\pi}\cdot\frac{0.005\cdot V_d}{r_c-1}\left[1+\frac{1}{2}(r_c-1)\left(R+1-\cos\theta-\sqrt{R^2-\sin^2\theta}\right)\right]}$$
$$\approx 7.15 \text{ mm},$$

where

V_d = displaced volume = 1600 cm^3
r_c = compression ratio = 7
θ = crank angle = 15°
R = ratio of connecting rod to crank radius = 260/70,

has been used for the calculation. This calculation was applied to the data in Figure 17 and the result is shown in Figure 22, together with the laminar flame speed for iso-octane calculated at the engine conditions from data given in Refs. [29] and [30].

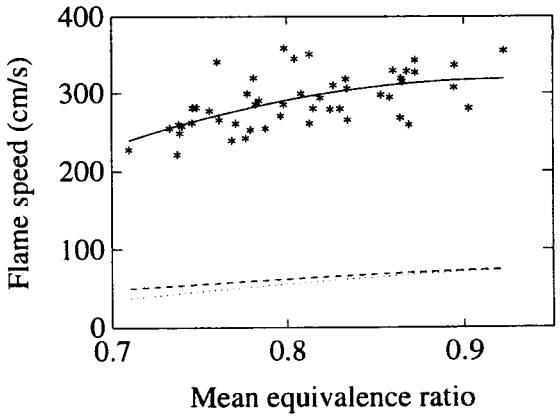

Figure 22 The mean burning speed (-) calculated from the data in Figure 17 is given together with the laminar flame speed calculated from Refs. [30] (--)and [29] (..).

According to an approximate burning law, [27], the burning speed should initially equal the laminar flame speed. After a time τ_b the flame has developed into a quasi-steady turbulent flame where the burning speed is given by

$$S_b = ku_T + S_L,$$

with S_L indicating the laminar flame speed and u_T the local turbulence intensity, k is a coefficient which depends on the flame size [31].

Figure 22 shows that the mean burning speed can be approximately expressed as

$$\bar{S}_b = S_L + C,$$

where C is on the order of 2 m/s. Comparison of the above expressions gives that C should be on the same order as the turbulence intensity. This in turn has been measured to be within, depending on operational parameters, the region of 1-3 m/s [26]. Hence, the calculated data is in reasonable agreement with what can be expected.

IMPROVEMENTS AND EXTENSIONS OF THE MEASUREMENT TECHNIQUE - The current primitive evaluation approach should be supplemented with a more sophisticated one, taking into account the effects of fuel concentration variations in the vicinity of the spark gap, for example by numerical simulation of a flame development based on the fuel concentration data. The minimum distance from the spark gap to the laser sheet is on the order of 3 mm. Influences from concentration variations on these length scales or less on the combustion instability can therefore not be investigated using the existing experimental data. The only way to remove this limitation is to use very thin electrodes by which the laser sheet can be positioned close to the spark gap. It might also be desirable to have a larger field of view, which is currently limited by engine design. If the fluorescence could be collected through a window in the piston, the fuel distribution across the entire cylinder cross-section could be obtained.

The significance of the statistical data derived from the measurements depends on the number of acquisitions. A correlation coefficent of 0.8 has, for instance, a 95% confidence interval between 0.66 to 0.88 with 50 samples [28]. Smaller statistical variations in the results can be expected if a larger number of engine cycles were acquired for each engine run. The acquisition of large measurement sequences necessitates the use of computers with very large data storage capacity and efficient backup equipment.

An interesting extension of the current measurement technique is to combine measurements of the concentration field by Laser-Induced Fluorescence, with simultaneous measurements of the velocity field by Laser Doppler Velocimetry. This combination has the potential of providing data explaining the major part of the combustion instability and would constitute a powerful tool for increased understanding of the underlying causes for the cyclic variations in spark-ignition engines.

CONCLUSIONS

1. Quantitative images of the fuel distribution within an operating engine were obtained using planar laser-induced fluorescence.
2. The fuel used iso-octane, does not fluoresce. To achieve fluorescence, a dopant is required. Three-pentanone was found to have vapour pressure characteristics comparable to those of iso-octane, as well as low absorption and suitable spectral properties.
3. A worst case estimation of the total accuracy from the PLIF images gives a maximum error of 0.03 in equivalence ratio.
4. An early injection timing gives a higher degree of charge inhomogenity close to the spark plug.
5. The charge inhomogenity with early injection gives a more unstable engine operation.
6. A correlation between combustion rate and average fuel concentration within a given radius from the spark plug center was identified on a cycle to cycle basis. When a second order polynomial was fitted, the correlation coefficient reached a value of ~0.8 with the engine running with a high degree of inhomogenity.
7. The highest correlation coefficient was obtained between the duration of 0-0.5% heat released and the average fuel concentration within a radius of approximately 5-10 mm from the spark plug.
8. When the standrd disc-shaped combustion chamber was replaced with a turbulence generating geometry, the inhomogeneity of the charge became very low, independent of injection timing. No cycle to cycle correlations between fuel/air equivalence ratio and combustion rate were then noted.

ACKNOWLEDGEMENTS

This work was part of CEC collaboration within the JRC-Homogeneous Combustion. We are indebted to this organisation as well as to the Swedish Board for Technical Development, NUTEK, for their financial support. We would also like to thank Dr. I. Magnusson, VOLVO AB, for his advice and helpful discussions.

REFERENCES

[1] C.L. Cummins "Internal Fire", Carnot Press, Lake Oswego, Oreg. (1976), which in turn refers to *N.A. Otto: German patent # 532.*

[2] Bosch "Automotive Handbook", Robert Bosch GmBH, Stuttgart, Germany (1986).

[3] O.Hoizinger, E. Linder "Ignition and Mixture Formation for Lean Burn Concepts", VDI Berichte 578, pp. 113-128 (in German) (1985).

[4] T.A. Baritaud, T.A. Heinze "Gasoline Distribution Measurements with PLIF in a SI Engine", SAE922355 (1992).

[5] F-Q. Zhau, M.Taketomi, K.Nishida, H. Hiroyasu "PLIF Measurements of the Cyclic Variations of Mixture Concentration in a SI Engine", SAE940988 (1994).

[6] T. Date, S. Yagi "Research and Development of the Honda CVCC Engine", SAE740605 (1974).

[7] A. C. Eckbreth,"Laser Diagnostics for Combustion Temperature and Species", Abacus Press, Cambridge (1987).

[8] D. R. Crosley and G. P. Smith "Laser-Induced fluorescence spectroscopy for combustion diagnostics", Opt. Eng. 22, 545 (1983).

[9] H. Neij, B.Johansson, and M. Aldé,n "Development and demonstration of 2D-LIF for studies of mixture preparation in SI engines", 25th Symp (Int) on Combustion (1994).

[10] M. Berckmllier, N.P. Tait, R.D. Lockett and D.A Greenhalgh, K. Ishii, Y. Urata, H. Umiyama and K. Yoshida, "In-Cylinder Crank Angle Resolved Imaging of Fuel Concentration in a Firing Spark-Ignition-engine using Planar LIFs", 25th Symp (Int) on Combustion (1994).

[11] F. Vannobel, A. Arnold, A. Buschmann, V. Sick, J. Wolfrum, B.Cousyn and M. Decker, "Simultaneuos Imaging of Fuel and Hydroxyl Radicals in an In-Line Four-Cylinder SI Engine", SAE932696 (1993).

[12] H. Neij,"Development of Laser-Induced Fluorescence for Combustion Diagnostics", Lund Reports on Combustion Physics LRCP-9, Licentiate thesis, Lund (1993).

[13] N.P. Tait and D.A. Greenhalgh, "2D laser-induced fluorescence imaging of parent fuel fraction in nonpremixed combustion", 24th Symp. (Int.) on Combustion; p. 1621, The Combustion Institute (1992).

[14] A. Arnold, H. Becker, R. Suntz, P. Monkhouse, J. Wolfrum, R. Maly and W. Pfister, "Flame front imaging in an internal-combustion engine simulator by laser-induced fluorescence of acetaldehyde", Opt. Lett. 15, 831 (1990).

[15] D. Wolff, V. Beushausen, H. Schlüter, P. Andresen, W. Hentschel, P. Manz, S. Arndt, "Quantitative 2D-Mixture Fraction Imaging Inside An Internal Combustion Engine Using Aceton-Fluorescence", International Symposium COMODIA 94 (1994).

[16] P.H. Paul, I. van Cruyningen, R.K. Hanson and G. Kychakoff,"High resolution digital flowfield imaging of jets", Exp. Fluids 9, 241 (1990).

[17] D.A. Stephenson, "Laser-Induced Fluorescence for High-Pressure Flow Visualization", Laser Institute of America ICALEO 42, 1 (1983).

[18] L.A. Melton, "Spectrally separated fluorescence emissions for diesel fuel droplets and vapor", Appl. Opt. 22, 2224 (1983).

[19] J.T. Hodges, T.A. Baritaud and T.A. Heinze, "Planar Liquid and Gas Fuel and Droplet Size Visualization in a DI Diesel Engine", SAE910726 (1991).

[20] C.H. Wang, X.Q. Liu and C.K. Law, "Combustion and Microexplosion of Freely Falling Multicomponent Droplets, Comb. Flame 56, 175 (1984).

[21] B.D. Smith and R. Srivastava, "Thermodynamic data for pure compounds. Part A, hydrocarbons and ketones", Elsevier (1986).

[22] D.A. Hansen and E.K.C. Lee, "Radiative and nonradiative transitions in the first excited singlet state of symmetrical methyl-substituted acetones", J. Chem. Phys. 62, 183 (1975).

[23] F. Ossler, To be published 1995.

[24] D.B. Leason, "The effect of gaseous additions on the burning velocity of propane-air mixtures", 4th Symp. (Int.) on Combustion; p. 369, The Combustion Institute (1952).

[25] K. Marforio, B. Lassesson and B. Johansson Influence of Flow Parameters and Spark Characteristics on the Early Flame Development in a SI-Engine", The 3rd Int Symposium on diagn. and model. of combustion in ICE, COMODIA94, Yokohama (1994)

[26] B. Johansson, "Correlation between velocity parameters measured with cycle-resolved 2-D LDV and early combustion in a spark ignition engine", Licenciate thesis, Report ISRN LUTMDN/TMVK--7012-SE, Department of Heat and Power Engineering, Lund Institute of Technology (1993).

[27] J.B. Heywood," Internal Combustion Engine Fundamentals", McGraw-Hill (1988).

[28] N.R. Draper and H. Smith, "Applied Regression Analysis", John Wiley & Sons (1981).

[29] M. Metghalchi and J.C. Keck, "Burning Velocities of Mixtures of Air with Methanol, Isooctane, and Indolene at High Pressure and Temperature", Comb. Flame 48, 191 (1982).

[30] Ö.L. Glder, "Laminar Burning Velocities of Methanol, Isooctane and Isooctane/Methanol blends", Combust. Sci. and Techn. 33, 719 (1983).

[31] M.D. Checkel and D. S-K. Ting, "Turbulence Effects on Developing Turbulent Flames in a Constant Volume Combustion Chamber", SAE930867 (1993).